

Reactively sintered porous MgAl₂O₄ for water-purification filter with controlled particle morphology

Yoko Kamato^a, Yoshikazu Suzuki^{a,b*}

^a Graduate School of Pure and Applied Sciences, University of Tsukuba, 1-1-1 Tennodai, Tsukuba, Ibaraki, 305-8573, Japan

^b Faculty of Pure and Applied Sciences, University of Tsukuba, 1-1-1 Tennodai, Tsukuba, Ibaraki, 305-8573, Japan

Abstract

Porous MgAl₂O₄ filters were prepared by reactive sintering of a MgCO₃ (basic) powder and 4-type Al₂O₃ source powders with different particle size and phases (α -Al₂O₃, fine and coarse boehmite AlOOH, and γ -Al₂O₃). The mixed powder compacts were reactively sintered in air at 1200, 1400 or 1600 °C for 2 h to obtain MgAl₂O₄. Single-phase porous MgAl₂O₄ was successfully obtained by the reactive sintering at 1400 and 1600 °C. From the SEM observation, the initial particle sizes of Al₂O₃ sources strongly affected the final microstructure of porous MgAl₂O₄, rather than the phases of Al₂O₃ sources. The porous MgAl₂O₄ filter made from fine boehmite source exhibited good performance to remove submicron-sized colloidal particles (simulating bacteria) from a suspension. Possibility of the thermal recovery of porous MgAl₂O₄ filter was demonstrated.

Key-words:

* Corresponding author:
Division of Materials Science, Faculty of Pure and Applied Sciences,
University of Tsukuba, Ibaraki 305-8573, Japan
E-mail: suzuki@ims.tsukuba.ac.jp (Y. Suzuki)

A. Powders: solid state reaction; A. Sintering; B. Porosity; D: Spinel; E: Membranes;

MgAl₂O₄

1. Introduction

Magnesium aluminate spinel, MgAl₂O₄, is a naturally produced mineral with a space group of cubic $Fd\bar{3}m$ and has a characteristic equilateral octahedron of the spinel structure [1,2]. Sintered MgAl₂O₄ is studied as a stable insulator material in the field of high energy applications, *e.g.*, fission and fusion energy devices [3,4]. MgAl₂O₄ has a high melting point (~2378 K) [5], and therefore, dense and porous MgAl₂O₄ sintered bodies have been applied to refractories [6,7] and thermal insulators [8], respectively. Furthermore, by using the excellent chemical stability of MgAl₂O₄, it is also applied for catalysts [9] and catalyst supports [10]. Hence, it is expected that porous MgAl₂O₄ membranes can be utilized as thermally and chemically stable filters.

The drinking water we usually have is supplied after the water-purifying treatment. In a water purification facility, raw water is processed step by step and supplied to us as living water. The microfiltration, separating about 100-200 nm particles from colloidal suspension, is usually performed by ceramics or organic membranes [11-15]. Although the ceramic filters are generally more expensive than the organic ones, these filters have outstanding characteristics such as high thermal-shock resistance, corrosion/erosion resistance and higher mechanical properties (except tensile strength) [16,17]. The ceramics filters can be adapted to a variety of liquid even under unfavorable conditions. In addition, backwashing, chemical washing or heating treatment enable to make the ceramics filters using for a longer time than the organic ones. We have recently reported ceramic water-purification filters made of porous pseudobrookite-type Al₂TiO₅ [18] and MgTi₂O₅ [19] with rod-like grains. Although

pseudobrookite-type ceramics have an advantage of low bulk thermal expansion in heating or cooling process, their mechanical properties may be insufficient for plant-level water-filtration facilities.

In this study, MgAl_2O_4 with favorable mechanical properties and excellent chemical stability was focused as ceramics filters. The microstructure of MgAl_2O_4 was controlled by changing the Al_2O_3 sources with different particle size and phases. And then, MgAl_2O_4 filters suitable for microfiltration with different pore size and porosity were prepared and characterized.

2. Experimental procedures

2.1 Preparation of MgAl_2O_4 pellet samples

A MgCO_3 (basic) powder ($\text{Mg}_5(\text{CO}_3)_4(\text{OH})_2 \cdot 4\text{H}_2\text{O}$, hydromagnesite, 99.9% purity, Kojundo Chemical Laboratory Co. Ltd., Japan) was used as a MgO source, **because the emitted H_2O and CO_2 gases can act as intrinsic pore-forming agents (called as pyrolytic reactive sintering [20,21].)** As Al_2O_3 sources, 4-type of commercially available powders were used, viz., α - Al_2O_3 (99.99% purity, 0.18 μm , TM-D, Taimei Chemicals Co. Ltd.), AIOOH-C01 (0.1 μm Taimei Chemicals Co. Ltd, Japan) and AIOOH-C06 (0.7 μm Taimei Chemicals Co. Ltd, Japan), γ - Al_2O_3 (99.9% purity, 2-3 μm , Kojundo Chemical Laboratory Co. Ltd., Japan). Prior to ball-milling, weight fractions of gaseous spaces in the powders (i.e., total of emitting H_2O and CO_2) were determined by thermogravimetry and differential thermal analysis (TG-DTA). **Table 1** summarizes the 4-type of mixed powders. MgCO_3 (basic) and Al_2O_3 -source powders (nominally, $\text{Mg}:\text{Al} = 1:1$ in mole fraction) were wet-ball milled in ethanol for 24 h. The mixed slurries were vacuum dried, and put it oven at 80°C for overnight. The mixed powders were then sieved through a 150-mesh screen. These starting mixtures with differing Al_2O_3 sources

were uniaxially pressed at 12 MPa for 1 min to obtain green compacts with dimension of ~15 mm in diameter and ~8 mm in thickness. The compacts were reactively sintered in air at 1200, 1400 or 1600 °C for 2 h (ramp rate: 5 °C/min) to obtain MgAl₂O₄, because our preliminary high-temperature XRD study (not shown) indicated that MgAl₂O₄ phase was synthesized at around 1100 °C. Additionally, 32 mmΦ compacts were prepared by the same procedure for the filtration test.

2.2 Characterization

The sintered pellets were pulverized and identified the resulting phases by using X-ray diffraction (XRD, Multiflex, Cu-Kα, 40 kV and 40 mA, Rigaku). The microstructure of the fracture surface was observed by scanning electron microscopy (SEM, SU-70, Hitachi and JSM-5600LV, JEOL). The bulk densities of the MgAl₂O₄ pellets were calculated by dimension and mass.

The filtration test was carried out by a lab-made filtration tester with a dead-end setup (Fig. 1). To prepare the colloidal suspension, AlOOH powder (Boehmite (C06), 0.7 μm, Taimei Chemicals Co. Ltd, Japan), simulating the typical bacteria size, was dispersed into distilled water with a dispersant (Sodium polyacrylate, T-50, Toagosei Group, Japan). The turbidity and pH of colloidal suspensions before and after filtration were measured by a portable turbidity meter (TN100R, Eutech Instruments, Singapore) and a portable pH meter (calibrated with pH 4 and pH 10 standard buffer solutions), respectively. The compressive strength was measured for some selected samples with a prismatic shape (typical dimension of ~4×4×12 mm) according to the JIS-R1608 standard.

The pore-size distribution was determined by mercury intrusion porosimetry (PoreMaster-60-GT, Quantachrome). Washburn equation was used to calculate the pore size,

where mercury surface tension is 480 dyne/cm and mercury contact angle is 140° [18].

3. Results

3.1 Phase analysis and microstructure

Figure 2 shows XRD patterns of the samples reactively sintered from 4-type mixed powders. For all 4 samples, substantially single-phase MgAl_2O_4 was obtained by the reactive sintering. At 1200 °C, a small amount of MgO and $\alpha\text{-Al}_2\text{O}_3$ were observed for some samples, but these peaks became negligible with increasing the sintering temperature.

Figure 3 shows the the bulk density and the porosity of samples sintered at 1200-1600 °C. The porosity values were nominally calculated from the measured bulk density (Fig. 3(a)) and the theoretical density of MgAl_2O_4 spinel (3.58 g/cm³), since the constituent phase was substantially single-phase MgAl_2O_4 as shown in Fig. 2. At 1200 °C, the density of all 4 samples was ~1.0 g/cm³, corresponding to the porosity of ~70%. At 1400 °C, the sample from MgAl-01, i.e. finer boehmite powder as Al_2O_3 source, became much denser than other 3 samples. The porosity of the MgAl-01 sample was ~50%, and that of others was ~ 65%. At 1600 °C, the sample from MgAl- α , i.e. highly sinterable $\alpha\text{-Al}_2\text{O}_3$ powder as Al_2O_3 source, was densified similarly to the sample from MgAl-01, corresponding to the porosity of ~23%. Considering the filter application, the samples sintered at 1200 °C seem to lack mechanical strength, and the sample sintered at 1600 °C may lack sufficient porosity. Hence, the samples sintered at 1400 °C were analyzed in the following part.

Figure 4 shows SEM images of the fracture surface of MgAl_2O_4 samples sintered at 1400 °C. The samples from MgAl- α (Fig. 4(a)) and MgAl-07 (Fig. 4(c)) had similar fine microstructure. The sample from MgAl-01 (Fig. 4(b)) was composed of MgAl_2O_4 with a variety size of secondary particles, reflecting the hard agglomeration in the starting powder of fine

boehmite particles (0.1 μm). The sample from MgAl- γ (Fig. 4(d)) was composed of somewhat larger MgAl₂O₄ grains, also reflecting the initial particle size of γ -Al₂O₃ (2-3 μm). From the SEM observation, the initial particle sizes of Al₂O₃ sources strongly affected the final microstructure of porous MgAl₂O₄, rather than the phases of Al₂O₃ sources.

3.2 Filtration test

The filtration tests were carried out using the porous MgAl₂O₄ filters sintered at 1400 °C. The thickness of porous filters was ca. 1.5-1.8 mm. As shown in Fig. 1, to improve the filtration efficiency, vacuum filtration at 85 kPa was conducted. **Figure 5** shows the results of turbidity and pH measurements using the porous filters, and **Fig. 6** depicts the filtration efficiency and porosity of the porous MgAl₂O₄ filters. Here, the filtration efficiency is defined as the volume of filtrated liquid (mL) per filtration time (min) per effective filter volume (cm³). For the MgAl- α sample, due to its insufficient mechanical strength, it cracked during the depressurization (Fig. 5 (a)), which is in good accordance with its small compressive strength of 6.3 ± 1.8 MPa (separately measured for prismatic samples). Note that we also tested the sample sintered at 1600 °C for the MgAl- α sample, but it did not function as a filter due to its low porosity of ~24%.

For the MgAl-01, MgAl-07 and MgAl- γ samples, the suspensions before and after the filtration are demonstrated in Fig. 5. With the MgAl-01 filter (Fig. 5(b)), although the filtration efficiency was low (0.20 mL/min·cm³), the reduction of turbidity was the highest (0.254 NTU), which even satisfies the water quality standards for drinking water in Japan, 2 NTU. The compressive strength of the MgAl-01 sample (porosity of ~48%) was 35.6 ± 4.3 MPa. Although this value was somewhat smaller than the porous MgAl₂O₄ by foam-gelcasting with spherical closed pores (52 MPa for porosity of 53.4%) in a recent report [22], it is still a high value for an

open porous 3-D network structure.

With the MgAl-07 filter (Fig. 5(c)), the reduction of turbidity was reasonably high (3.80 NTU), but it was lower than that of MgAl-01 despite the higher porosity of 65.3%, which implies an abundance of closed (or inaccessible) pores in the MgAl-07 filter. With the MgAl- γ filter (Fig. 5(d)), filtration efficiency was the highest due to its coarse microstructure (as shown in Fig. 2(d)), but the reduction of turbidity became the lowest (22.9 NTU). The results of pH measurement well support the results of turbidity measurement, i.e., the reduction of pH values (almost neutral) after the filtration.

3.3 Mercury porosimetry

In order to understand the different filtration ability among the MgAl-01, MgAl-07 and MgAl- γ samples, mercury porosimetry test was conducted. **Figure 7** shows the pore-size distributions and **Table 2** summarizes the analysis results of mercury porosimetry. In good agreement with the SEM observation (Fig. 4) and the turbidity measurement (Fig. 5), the MgAl- γ sample contained larger pores than MgAl-01 and MgAl-07 samples. The pore volume per solid mass of MgAl-01 estimated from the mercury porosimetry is about half of that of MgAl- γ (Fig. 7(a)). The three pore-size peaks of MgAl-01 in Fig. 7(b) correspond to the existence of a variety size of secondary particles, reflecting the hard agglomeration in the starting powder of fine boehmite particles (0.1 μm).

4. Discussion

Here we discuss the relationship between microstructure and filter performance. **Figure 8** schematically illustrates the microstructure of the porous samples. Since the dead-end type setting was used in this study, the colloid particles (0.7 μm) tended to form thick cake layer on

the filter surfaces, particularly on the MgAl-01 and the MgAl-07 samples (**Fig. 9**). The cake layer was effective to reduce the turbidity (Fig. 5), but it decreased the filtration efficiency (as shown in Fig. 6). Meanwhile, on the MgAl- γ surface, the cake layer was not as thick as MgAl-01/07 samples, due to the larger open pore-size. Comparing MgAl-01 and MgAl-07, the filtration efficiency of MgAl-07 was very low, suggesting the small open-pore channel size or abundant closed (or inaccessible) porosity (Fig. 8). **Actually, the mercury porosimetry (Fig. 7(b) and Table 2) showed that the mode pore sizes of MgAl-01 and MgAl-07 were 660 and 211 nm, respectively. These data indicate that MgAl-01 contained somewhat thicker open-pore channel compared with MgAl-07.**

By using the total pore volume per solid mass determined by the mercury porosimetry (0.250, 0.466 and 0.490 cm³/g for MgAl-01, MgAl-07 and MgAl- γ) in Table 2, and the theoretical density of MgAl₂O₄ spinel (3.578 g/cm³, viz., 0.2795 cm³/g), the open porosity (i.e., for pores that are accessible by intruding mercury) can be calculated to be 47.2%, 62.5% and 63.7%, respectively. They are close to those of the nominal porosity calculated from dimension and mass. Taking into account error factors of porosity measurements (for both by dimension-mass and mercury intrusion), e.g., individual difference of samples, approximation of single phase composition, sample contour distortion, humidity etc., here we can deduce that most of the pores in these samples should be open (for pressurized mercury), and the closed porosity in these samples can be estimated to be less than several %. Still, we should recall that finer pores (in particular for MgAl-07) cannot be accessed by water-based suspension under the near-ambient pressure.

5. Conclusions

In this paper, reactively sintered porous MgAl₂O₄ was studied as a water purification filter.

The porous microstructure of MgAl_2O_4 was controllable just by changing the Al_2O_3 sources with different particle size and phases. The porous MgAl_2O_4 filter made from fine boehmite source exhibited good performance to remove submicron-sized colloidal particles (simulating bacteria) from a suspension. Possibility of the thermal recovery of porous MgAl_2O_4 filter was demonstrated.

Acknowledgment

This work is supported by Nippon Sheet Glass Foundation for Materials Science and Engineering. We thank to Prof. Tamotsu Koyano at University of Tsukuba for the help of SEM observation.

References

- [1] T. H. Nielsen, M. H. Leipold, Thermal expansion in air of ceramic oxides to 2200°C, *J. Am. Ceram. Soc.* 46 (1963) 381–387.
- [2] K. E. Sickafus, J. M. Wills, N. W. Grimes, Structure of spinel, *J. Am. Ceram. Soc.* **82** (1999) 3279–3292.
- [3] S. J. Zinkle, G.P. Pells, Microstructure of Al₂O₃ and MgAl₂O₄ irradiated at low temperatures, *J. Nucl. Mater.* 253 (1998) 120–132.
- [4] G. Szenes, Ion-induced amorphization in ceramic materials, *J. Nucl. Mater.* 336 (2005) 81–89.
- [5] B. Hallstedt, Thermodynamic assessment of the system MgO-Al₂O₃, *J. Am. Ceram. Soc.* 75 (1992) 1497–1507.
- [6] D. Schmidtmeier, G. Büchel, A. Buhr, Magnesium aluminate spinel raw materials for high performance refractories for steel ladles, *Ceram. Mater.* 61 (2009) 223–227.
- [7] W. S. Resende, R. M. Stoll, E. M. J. A. Pallone, F. N. Cunha, R. C. Bradt, Spinel refractory aggregates from natural raw materials, *Miner. Met. Process.* 18 (2001) 68–74.
- [8] S. Hashimoto, S. Honda, T. Hiramatsu, Y. Iwamoto, Fabrication of porous spinel (MgAl₂O₄) from porous alumina using a template method, *Ceram. Int.* 39 (2013) 2077–2081.
- [9] J. I. Di Cosimo, V. K. Díez, M. Xu, E. Iglesia, C. R. Apesteguía, Structure and surface and catalytic properties of Mg-Al basic oxides, *J. Catal.* 178 (1998) 499–510.
- [10] J. Guo, H. Lou, H. Zhao, X. G. Wang and X. M. Zheng, Novel synthesis of high surface area MgAl₂O₄ spinel as catalyst support, *Mater. Lett.* 58 (2004) 1920-1923.
- [11] A. Lonigro, A. Pollice, R. Spinelli, F. Berrilli, D. Di Cave, C. D’Orazi, P. Cavallo, O. Brandonisio, *Giardia* cysts and *cryptosporidium* oocysts in membrane-filtered municipal

- wastewater used for irrigation, *Appl. Environ. Microbiol.* 72 (2006) 7916–7918.
- [12] J. Ottosona, A. Hansena, B. Bjöleniusc, H. Norderd, T. A. Stenströma, Removal of viruses, parasitic protozoa and microbial indicators in conventional and membrane processes in a wastewater pilot plant, *Water Res.* 40 (2006) 1449–1457.
- [13] O. Nkwonta, G. Ochieng, Roughing filter for water pre-treatment technology in developing countries: A review, *Int. J. Phys. Sci.* 4 (2009) 455–463.
- [14] S.-L. Loo, A. G. Fane, W. B. Krantz, T.-T. Lim, Emergency water supply: a review of potential technologies and selection criteria, *Water Res.* 46 (2012) 3125–3151.
- [15] J. M. Dickhout, J. Moreno, P. M. Biesheuvel, L. Boels, R. G. H. Lammertink, W. M. de Vos, Produced water treatment by membranes: A review from a colloidal perspective, *J. Colloid Interface Sci.* 487 (2017) 523–534.
- [16] V. V. Goncharuk, D. D. Kucheruk, M. N. Balakina, T. Yu. Dul’neva, Water treatment by baromembrane methods based on ceramic membranes, *J. Water Chem. Technol.* 31 (2009) 396–404.
- [17] P. Wu, Y. Xu, Z. Huang, J. Zhang, A review of preparation techniques of porous ceramic membranes, *J. Ceram. Process. Res.* 16 (2015) 102–106.
- [18] T. Hono, N. Inoue, M. Morimoto, Y. Suzuki, Reactive sintering and microstructure of uniform, openly porous Al_2TiO_5 , *J. Asian Ceram. Soc.* 1 (2013) 178–183.
- [19] Y. Nakagoshi, Y. Suzuki, Pseudobrookite-type MgTi_2O_5 water purification filter with controlled particle morphology, *J. Asian Ceram. Soc.*, 3 (2015) 334–338.
- [20] Y. Suzuki and P. E. D. Morgan, Meso- and macroporous ceramics by phase separation and reactive sintering methods, *MRS Bull.* 34 (2009) 587-591.
- [21] Y. Suzuki, T. S. Suzuki, Y. Shinoda, and K. Yoshida, Uniformly porous MgTi_2O_5 with narrow pore-size distribution: XAFS study, improved in-situ synthesis, and new in-situ

surface coating, *Adv. Eng. Mater.* 14 (2012) 1134-1138.

- [22] X. Deng, J. Wang, J. Liu, H. Zhang, L. Han, S. Zhang., Low cost foam-gelcasting preparation and characterization of porous magnesium aluminate spinel ($MgAl_2O_4$) ceramics, *Ceram. Int.* 42 (2016) 18215-18222.

Tables

Table 1 Mixed powders with different Al_2O_3 sources in this study.

| Sample name (mixed powder) | Raw materials | |
|-------------------------------|----------------------------------|----------------------------------|
| | MgO source | Al_2O_3 source |
| MgAl- α | $Mg_5(CO_3)_4(OH)_2 \cdot 4H_2O$ | $\alpha-Al_2O_3$ (0.18 μm) |
| MgAl-01 | $Mg_5(CO_3)_4(OH)_2 \cdot 4H_2O$ | AlOOH (0.1 μm) |
| MgAl-07 | $Mg_5(CO_3)_4(OH)_2 \cdot 4H_2O$ | AlOOH (0.7 μm) |
| MgAl- γ | $Mg_5(CO_3)_4(OH)_2 \cdot 4H_2O$ | $\gamma-Al_2O_3$ (2~3 μm) |

Table 2 Mercury porosimetry analysis for porous $MgAl_2O_4$ samples.

| Sample name | Sample mass [g] | Total pore volume [cm^3/g] | Specific surface area [m^2/g] | Average pore diameter [nm] | Mode pore diameter [nm] | Median pore diameter [nm] |
|----------------|-----------------|--------------------------------|-----------------------------------|----------------------------|-------------------------|---------------------------|
| MgAl-01 | 0.4788 | 0.250 | 10.45 | 93.97 | 660.00 | 142.80 |
| MgAl-07 | 0.4618 | 0.466 | 18.43 | 98.81 | 211.10 | 191.60 |
| MgAl- γ | 0.4533 | 0.490 | 6.47 | 300.80 | 666.70 | 595.90 |

Figure captions

- Fig. 1** Filtration device set-up.
- Fig. 2** XRD patterns of the samples reactively sintered at (a) 1200, (b) 1400 and (c) 1600 °C.
- Fig. 3** Density and nominal porosity of the sample reactively sintered at 1200-1600 °C. Nominal porosity was calculated from the measured density and the theoretical density of MgAl₂O₄ spinel, 3.58 g/cm³.
- Fig. 4** SEM images of the fracture surface of MgAl₂O₄ samples reactively sintered at 1400 °C: (a) MgAl- α , (b) MgAl-01, (c) MgAl-07 and (d) MgAl- γ .
- Fig. 5** Turbidity and pH measurements using porous samples sintered at 1400°C: (a) MgAl- α sample was broken during filtration due to insufficient mechanical strength. (b)-(d) Suspensions before and after filtration: (b)MgAl-01, (c) MgAl-07 and (d) MgAl- γ .
- Fig. 6** Filtration efficiency and porosity of the porous MgAl₂O₄ samples. The porosity values are for the porous filter discs (32 mm ϕ in green compacts).
- Fig. 7** Pore-size distributions determined by mercury porosimetry: (a) cumulative pore volume and (b) differential pore volume, $dV/d(\log D)$.
- Fig. 8** Schematic illustration of the porous microstructure derived from SEM observation.
- Fig. 9** SEM micrographs on the filter surface before and after the filtration.

Figures

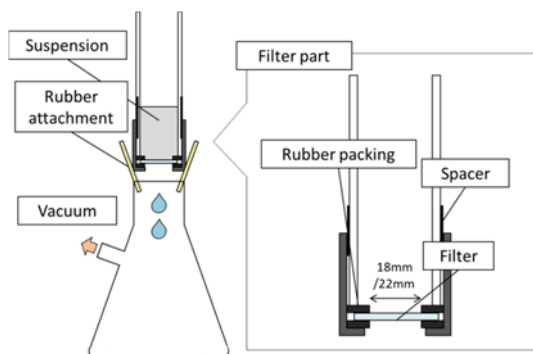


Fig. 1 Filtration device set-up.

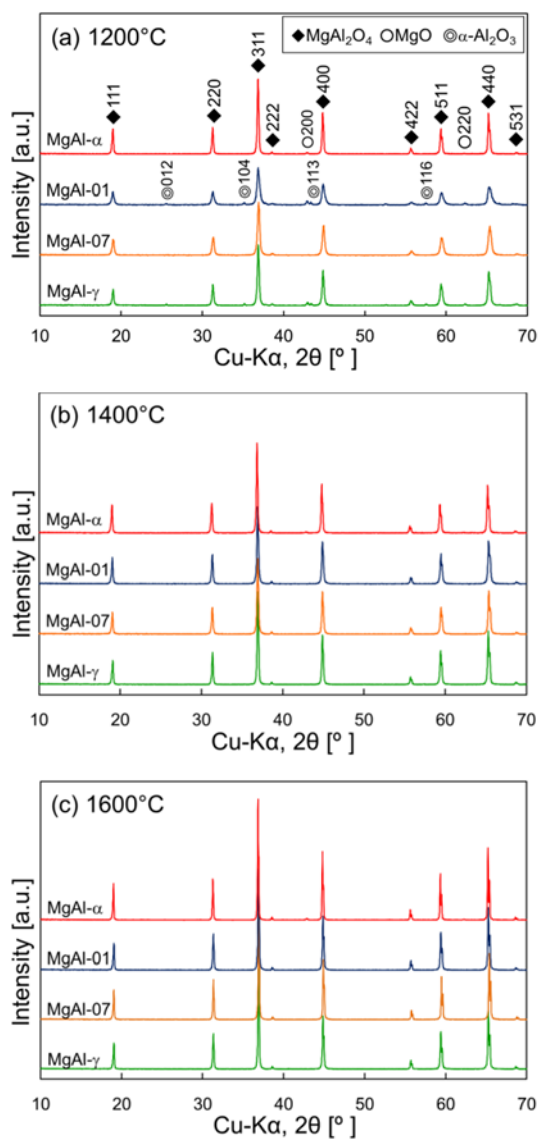


Fig. 2 XRD patterns of the samples reactively sintered at (a) 1200, (b) 1400 and (c) 1600 °C.

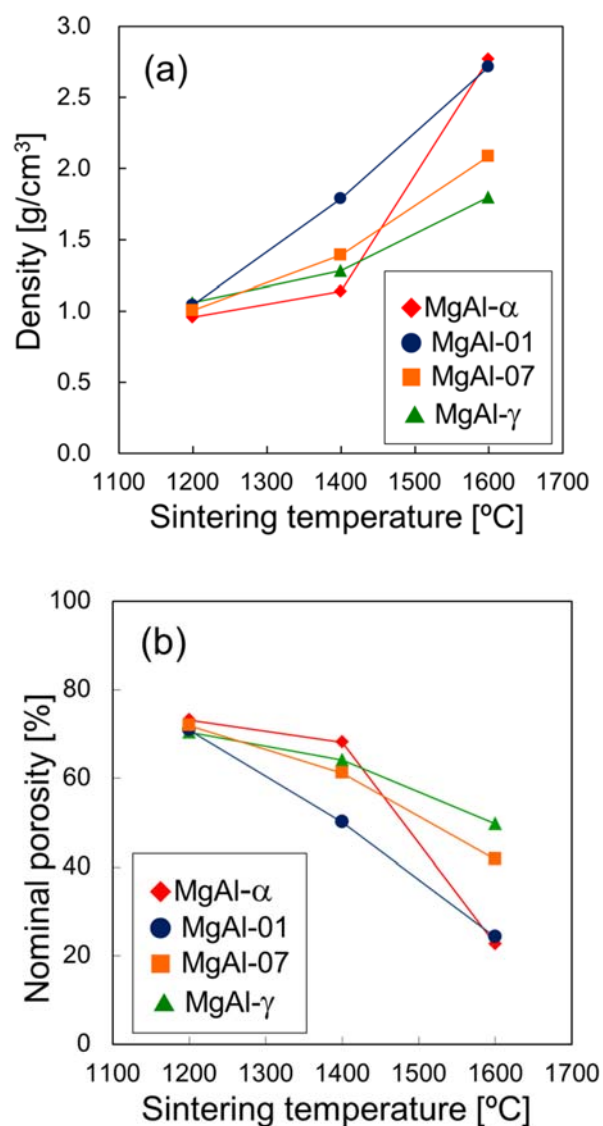


Fig. 3 Density and nominal porosity of the sample reactively sintered at 1200-1600 °C. Nominal porosity was calculated from the measured density and the theoretical density of MgAl₂O₄ spinel, 3.58 g/cm³.

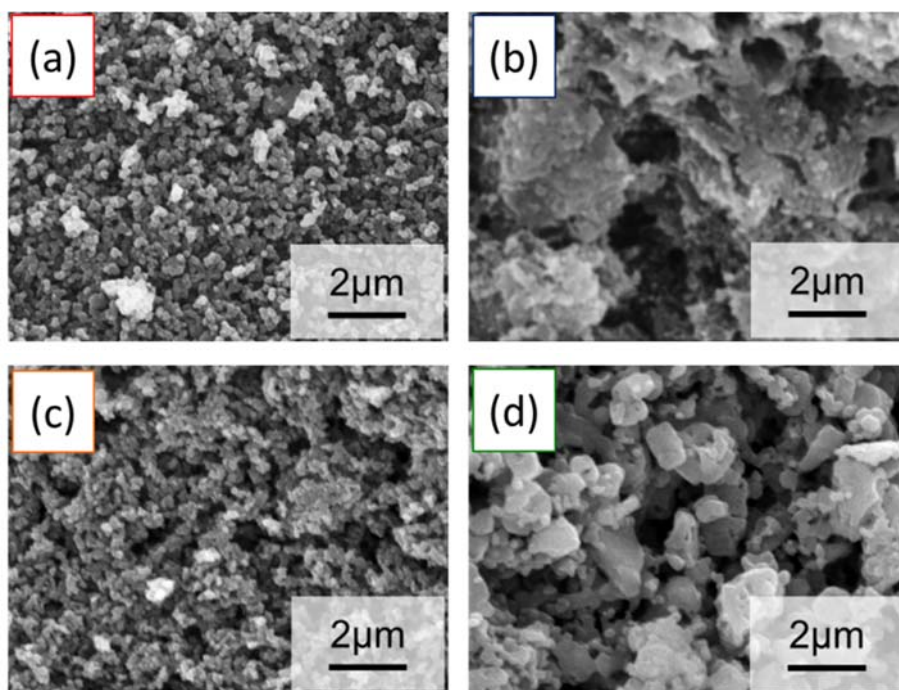


Fig. 4 SEM images of the fracture surface of MgAl₂O₄ samples reactively sintered at 1400 °C: (a) MgAl- α , (b) MgAl-01, (c) MgAl-07 and (d) MgAl- γ .

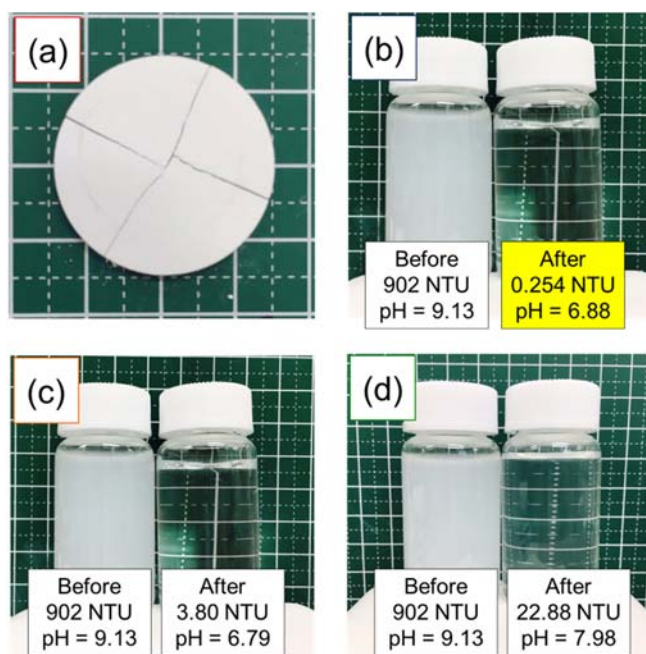


Fig. 5 Turbidity and pH measurements using porous samples sintered at 1400°C: (a) MgAl- α sample was broken during filtration due to insufficient mechanical strength. (b)-(d) Suspensions before and after filtration: (b)MgAl-01, (c) MgAl-07 and (d) MgAl- γ .

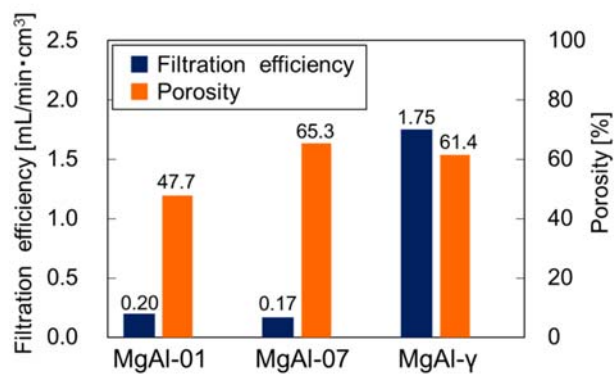


Fig. 6 Filtration efficiency and porosity of the porous MgAl₂O₄ samples. The porosity values are for the porous filter discs (32 mmφ in green compacts).

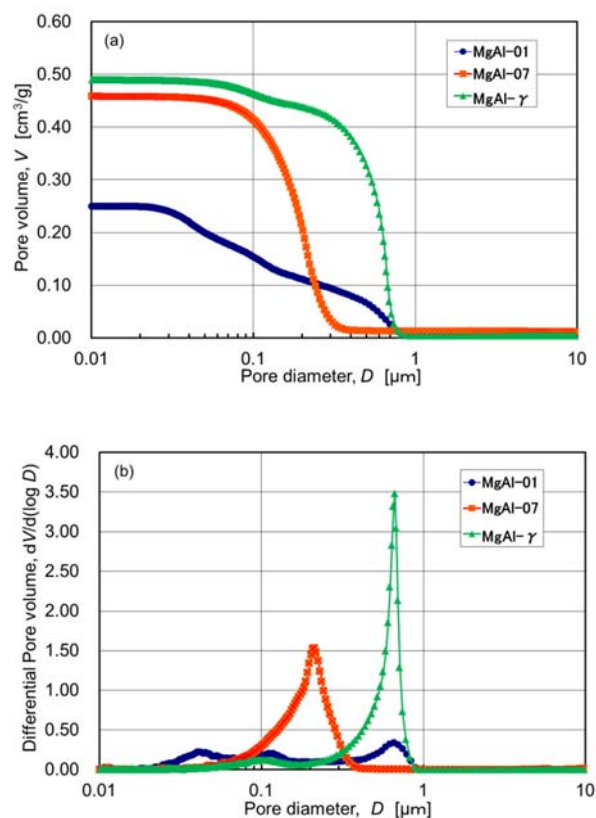


Fig. 7 Pore-size distributions determined by mercury porosimetry: (a) cumulative pore volume and (b) differential pore volume, $dV/d(\log D)$.

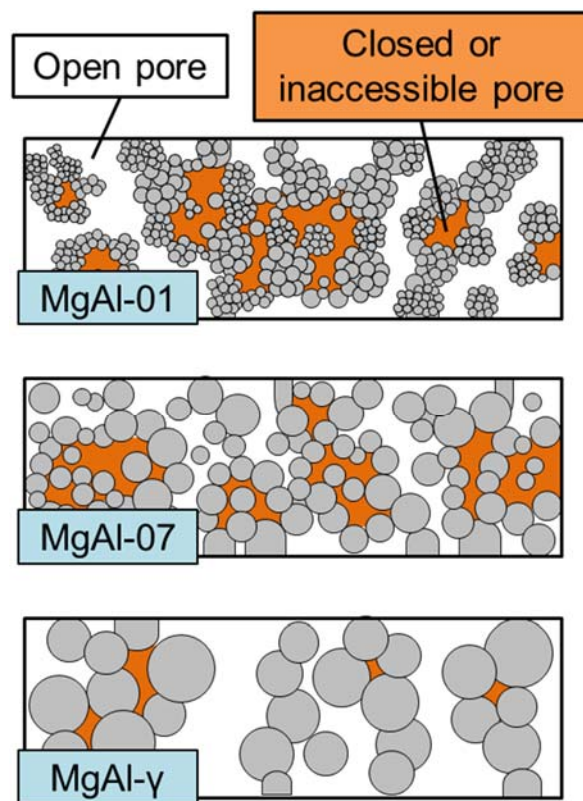


Fig. 8 Schematic illustration of the porous microstructure derived from SEM observation.

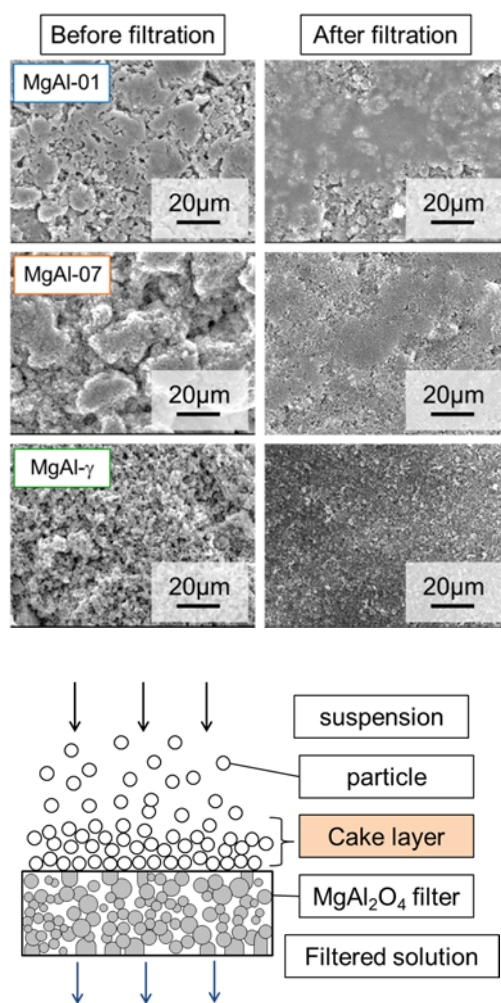


Fig. 9 SEM micrographs on the filter surface before and after the filtration.

Supporting information

The recyclability of MgAl_2O_4 filters were evaluated by a similar filtration test but using an Indian ink as colloidal suspension. Filters after filtration were calcined at 1000°C for 1 h to thermally decompose the organic material. The appearance and the XRD pattern of the filter after thermal recovery were almost unchanged from those of the filter before filtration as shown in Fig. S1.

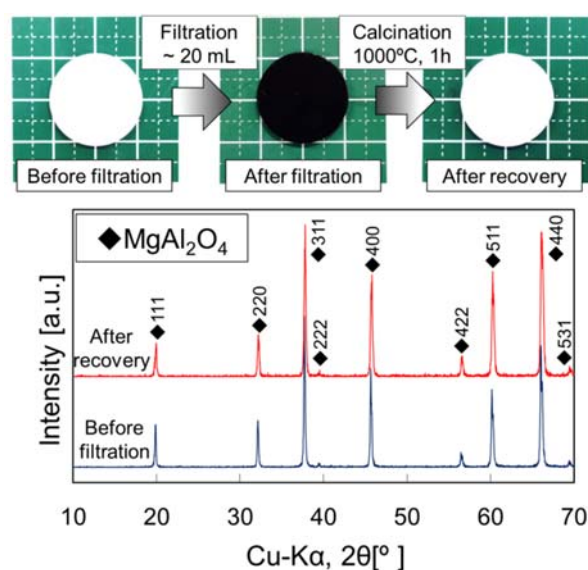


Fig. S1 Filtration of Indian ink (colloidal carbon suspension) using the sample sintered at 1400°C from the MgAl -01 mixed powder, and filter recovery test by the calcination at 1000°C for 1 h.